Editors' Suggestion

Solid-Liquid Transition of Deformable and Overlapping Active Particles

Benjamin Loewe,[1,*] Michael Chiang,[2] Davide Marenduzzo,[2] and M. Cristina Marchetti[1]
[1]Department of Physics, University of California Santa Barbara, Santa Barbara, California 93106, USA
[2]SUPA, School of Physics and Astronomy, University of Edinburgh, Peter Guthrie Tait Road, Edinburgh EH9 3FD, United Kingdom

(Received 27 December 2019; revised 24 April 2020; accepted 16 June 2020; published 15 July 2020)

Experiments and theory have shown that cell monolayers and epithelial tissues exhibit solid-liquid and glass-liquid transitions. These transitions are biologically relevant to our understanding of embryonic development, wound healing, and cancer. Current models of confluent epithelia have focused on the role of cell shape, with less attention paid to cell extrusion, which is key for maintaining homeostasis in biological tissue. Here, we use a multiphase field model to study the solid-liquid transition in a confluent monolayer of deformable cells. Cell overlap is allowed and provides a way for modeling the precursor for extrusion. When cells overlap rather than deform, we find that the melting transition changes from continuous to first order like, and that there is an intermittent regime close to the transition, where solid and liquid states alternate over time. By studying the dynamics of five- and sevenfold disclinations in the hexagonal lattice formed by the cell centers, we observe that these correlate with spatial fluctuations in the cellular overlap, and that cell extrusion tends to initiate near fivefold disclinations.

DOI: 10.1103/PhysRevLett.125.038003

Understanding the dynamics and collective behavior of cells in dense tissues is an important goal of biophysics, with relevance to a number of developmental processes, such as embryogenesis [1], wound healing [2], and cancer [3]. For example, the epithelial-mesenchymal transition can be viewed as a solid-liquid transition occurring *in vivo* [4–6], where cells become more motile and less adhesive: this transition has been reported to play a role in tissue repair, inflammation, and tumor progression [3,7,8]. Experimental studies have also shown that epithelial cells can undergo an unjamming transition between a glassy phase where their dynamics is slow to a fluid phase with large-scale collective motion both *in vitro* [9–14] and *in vivo* [14,15].

From a theoretical point of view, an appealing model of a dense tissue is provided by a two-dimensional (2D) confluent cell monolayer (i.e., a space-filling cell monolayer with packing fraction equal to unity). This system can be studied by the cellular Potts model [16], the vertex [17–20] and Voronoi [21,22] models, and their variants [23,24]. Such frameworks have recently been used to study the melting transition in monolayers of passive [20,25,26] and active (motile) cells [22,27–29]. Cell motility and deformability distinguish this problem from the 2D melting of crystals of hard or soft disks [30–33], which proceeds either via a discontinuous transition [34,35], or through an intermediate hexatic phase and the unbinding of topological defects [36–41].

Existing studies of vertex and Voronoi models of confluent active monolayers suggest that a continuous solid-liquid (or glass-liquid) transition can be observed upon increasing cell motility [22,28]. While useful in providing quantitative predictions, this work has mainly focused on the role of cell intercalation (T1 transitions) in controlling tissue rigidity and less on the role of cell extrusion that in these strictly 2D models may be described by cell removal (T2 transitions) [18,42]. In many situations, however, cell extrusion is driven by cell crowding and overlap, as commonly seen in confluent epithelia [43]. Cell overlap also occurs during early embryogenesis as an epithelial monolayer is converted into a multilayered epithelium following a tightly coordinated stratification program [44]. Here we consider a model that explicitly allows for cell overlap, interpreted as a precursor for cell extrusion, to examine its role on the solid-liquid transition of a confluent tissue.

To incorporate both particle deformation and overlap we use a multiphase field model [45–48] to study melting of a confluent layer of motile deformable particles. The behavior of our system is controlled by the trade-off between deformability and overlap: the less deformable a particle is, the more it overlaps with its neighbors. At high deformability we find a continuous solid-liquid transition with increasing cell motility. The transition becomes first order like at low deformability when cells overlap, with an intermediate intermittent state, where the system as a whole alternates between solid and liquid states. Finally, we observe a strong correlation between unbound structural defects (corresponding to five- and sevenfold disclinations in the hexagonal lattice formed by the cell centers) generated upon melting and local fluctuations in cell overlap. Specifically, we find that cellular extrusion is favored at fivefold disclinations.

Our model may also serve as a bridge between particle-based and confluent models. Upon decreasing cell deformability, the system transitions from deformable particles that tessellate their domain without overlap, similar to vertex models, to almost-circular overlapping disks. The connection with these two limiting cases is, however, only qualitative. At high deformability, anisotropy of cell shape is strongly correlated with fluidity (Figs. S5 and S6 [49]), but, unlike vertex models, it does not provide an order parameter for the liquid state. Conversely, at low deformability, overlap in our model is much higher than that allowed in systems of soft disks.

Our multiphase field model contains N scalar fields, $\{\phi_i(\boldsymbol{r})\}_{i=1}^{N}$, each representing a different cell. The equilibrium configuration of the cell layer is determined by the minimization of the following free energy [46,48]:

$$\mathcal{F} = \sum_{i=1}^{N}\left[\int d^2\boldsymbol{r}\left(\frac{\alpha}{4}\phi_i^2(\phi_i-\phi_0)^2+\frac{K}{2}(\nabla\phi_i)^2\right)\right.$$
$$\left.+\lambda\left(1-\int d^2\boldsymbol{r}\frac{\phi_i^2}{\pi R^2\phi_0^2}\right)^2+\varepsilon\sum_{i<j=1}^{N}\int d^2\boldsymbol{r}\phi_i^2\phi_j^2\right]. \quad (1)$$

The first three terms determine the shape of the cells. The first term sets ϕ_0 and zero as the preferred values of the field inside and outside the cell, respectively. The second term penalizes spatial variations of ϕ. Together, they determine the physical properties of the cell boundary, such as the interfacial thickness, which we define as $\xi=\sqrt{2K/\alpha}$, and surface tension $\sigma=\sqrt{8K\alpha/9}$ [52]. The third term is a soft constraint that sets the preferred area of the cell to that of a circle with target radius R. Finally, the fourth term models the steric repulsion between cells by energetically penalizing cell overlap.

To model the dynamics of motile cells, we assume simple relaxational and overdamped dynamics,

$$\frac{\partial\phi_i}{\partial t}+\boldsymbol{v}_i\cdot\nabla\phi_i=-\frac{1}{\gamma}\frac{\delta\mathcal{F}}{\delta\phi_i}, \quad (2)$$

where γ is a friction coefficient and we have included an advection term that propels the cells with velocity $\boldsymbol{v}_i$, see [49]. All cells have the same propulsion speed v_0, while their direction of motion θ_i is controlled by rotational noise with diffusivity D_r,

$$d\theta_i(t)=\sqrt{2D_r}dW_i(t), \quad (3)$$

where W_i is a Wiener process. Cell motility is quantified by the Péclet number $\mathrm{Pe}\equiv(v_0/D_r)/R$, which is the ratio between the cells' persistence length and their target radius. These equations are a generalization of the active Brownian particle model [53,54] to a system of deformable cells.

Our model allows cells to both deform and overlap. In general, these are competing effects: deformation is energetically penalized by surface tension, while overlap is penalized by repulsion. We quantify cell deformability through the dimensionless ratio $d\equiv\varepsilon/\alpha$. When $d\ll 1$, cells tend to acquire a circular shape and overlap with their neighbors [Figs. 1(a), 1(c), and 1(e)]. Conversely, when $d\gg 1$, cells change their shape to match with their neighbors and minimize overlap [Figs. 1(b), 1(d), and 1(f)].

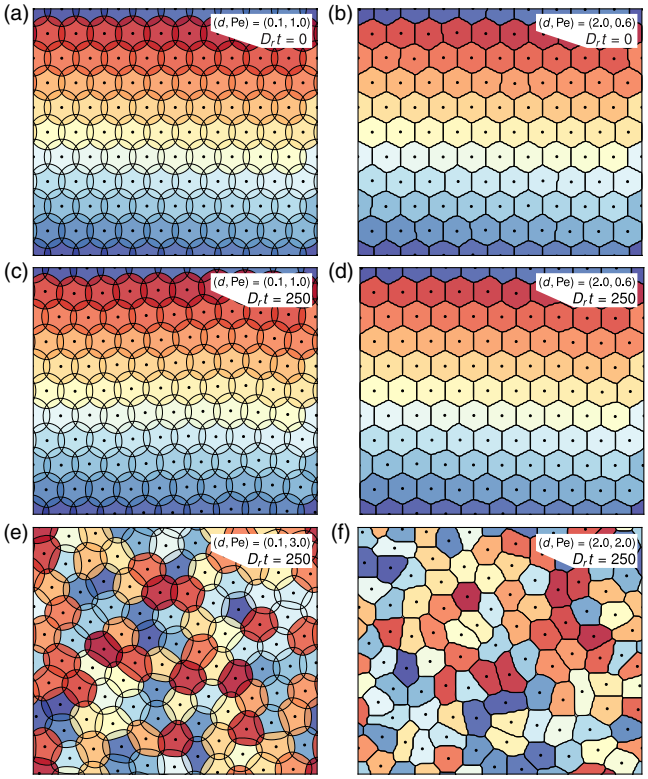

FIG. 1. Simulation snapshots of the stationary state for different deformability (quantified by d) and motility (quantified by Pe). The contours of the cells correspond to the level $\{\phi_i=1\}_{i=1}^{N}$, while the coloring corresponds to the cell index at $t=0$ (for visualizing cell rearrangements). (a), (b) The initial condition of the monolayer at (a) $d=0.1$ and (b) $d=2.0$. Note that cells overlap at low d, whereas at high d cells deform rather than overlap. (c)–(f) Snapshots of the system at $D_r t=250$. The system remains in a crystal-like state at low motility [(c), (d)]. At sufficiently high motility, the system melts and cells exchange neighbors [(e), (f)]. See also Supplemental Movies 1–4 [49].

We first examine the role of deformability and motility on the solid-liquid transition at confluence. To this end, we employ a finite difference method to solve numerically Eqs. (2) and (3) for $N=36$ and 100 cells in a rectangular box of aspect ratio that accommodates an undeformed hexagonal cell lattice, with periodic boundary conditions. Choosing R as unit of length and D_r^{-1} as unit of time, we use $\delta x=1/12$ and $\Delta t=5\times10^{-5}$ as our simulation lattice unit and time step, respectively. We tune deformability by varying α and K such that ξ is constant. We initiate the cells in a hexagonal lattice with $\lambda\geq 3000$ K and allow the system to achieve confluence by setting the cell target area

πR^2 to be larger than the area available to each cell. Further simulation details and the list of parameters are given in the Supplemental Material.

To quantify the melting transition, we compute both dynamical and structural observables [49]. Dynamical arrest is quantified through an effective diffusivity $\bar{D}_{\mathrm{eff}}$ [22,27] obtained from the long-time behavior of the mean square displacement $\mathrm{MSD}(t)$ of individual cells as $\bar{D}_{\mathrm{eff}} = \lim_{t\to\infty} \mathrm{MSD}(t)/(4D_0 t)$, with $D_0 = v_0^2/(2D_r)$ the diffusivity of an isolated cell. As structural observables, we measure the global bond-orientational order parameter $|\Psi_6|$ and the structure factor $S(\boldsymbol{q})$. Choosing $\bar{D}_{\mathrm{eff}} > 0.0005$ as the threshold for a liquid state, the transition lines obtained from the dynamical and structural measurements coincide. The phase diagram displayed in Fig. 2 shows that both deformability and motility facilitate melting. We also find a region of intermittence at low deformability, discussed further below. The width of the plateau in the MSD at intermediate times shrinks with increasing deformability, suggesting that deformability facilitates melting by allowing particles to squeeze more easily through the cages provided by their neighbors.

One of our key results is that the nature of the transition is different at low and high deformability. This can be appreciated by analyzing the standard error of $|\Psi_6|$ across the parameter space (d, Pe), which shows that there is an intermediate Pe range at $d < 1$ for which this quantity is large. Intriguingly, $d < 1$ is precisely the region in parameter space where the overlap between cells becomes appreciable, implying that the character of monolayer melting depends on whether the rearrangement of particles occurs by cells squeezing past their neighbors by deforming ($d > 1$) or crawling over them by overlapping ($d < 1$).

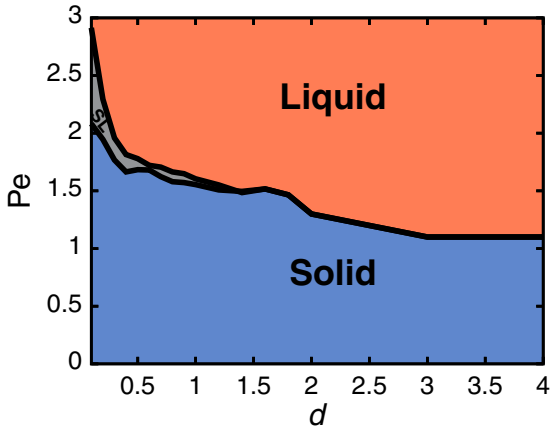

FIG. 2. Phase diagram of melting in our confluent system. The transition lines separating the solid, intermittent (labeled as SL), and liquid phases are interpolation of the boundaries identified based on the system's diffusivity $\bar{D}_{\mathrm{eff}}$, its global bond-orientational order $|\Psi_6|$, and the fraction of structural defects $\langle|\Delta N_{\mathrm{nn}}|\rangle$ in the system.

To determine the nature of the intermediate regime found at $d < 1$, we analyze the corresponding time series of $|\Psi_6|$ [Fig. 3(a)]. The time series shows clear evidence of an intermittent behavior, where the system jumps between two distinct states with different mean values of $|\Psi_6|$ (see also Supplemental Movie 5 [49]). The two states are also apparent from the bimodal character of the $|\Psi_6|$ probability density function [PDF; Fig. 3(d)]. Since $|\Psi_6|$ correlates with the melting transition and our solid state is close to a hexagonal crystal, we can associate $|\Psi_6| \simeq 1$ to a solid state, and values of $|\Psi_6|$ close to or below 0.5 to a liquid state. Moreover, the values of $|\Psi_6|$ in the solid and liquid regimes fluctuate around well-defined means, and hence exhibit unimodal PDFs (albeit with different widths), so that bimodality in the PDF signals intermittence. We also identify intermittence by computing the fraction of defects in the system $\langle|\Delta N_{\mathrm{nn}}|\rangle$ [Figs. 3(b) and 3(c)], i.e., the fraction of the total number of cells with a coordination number other than six. The time series for $\langle|\Delta N_{\mathrm{nn}}|\rangle$ shows that defects appear when the monolayer is in the liquid state. In addition, and in line with Ref. [33], we observe that defects in the intermittent phase tend to

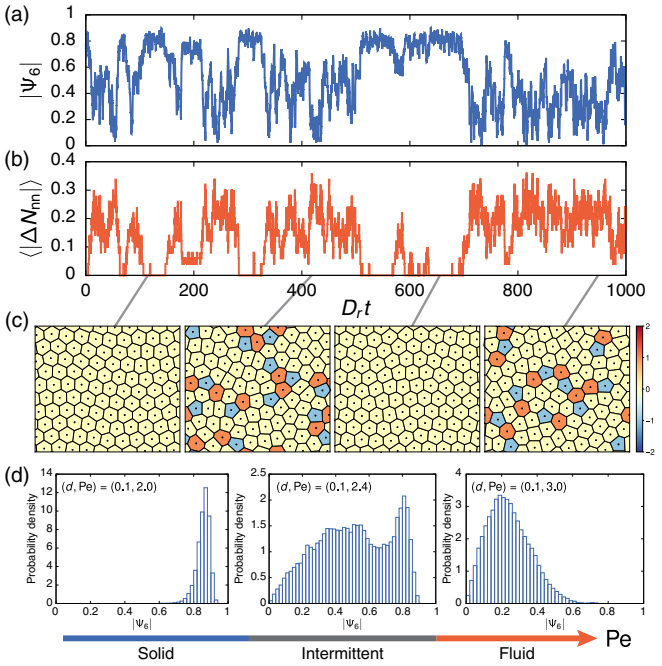

FIG. 3. Intermittence at low deformability. (a)–(c) Intermittent behavior at $(d, \mathrm{Pe}) = (0.1, 2.4)$. (a) Time series of $|\Psi_6|$. (b) Time series of the fraction of defects $\langle|\Delta N_{\mathrm{nn}}|\rangle$. (c) Voronoi tessellation of the system depicting instantaneous configurations in the solid and liquid states, and highlighting the presence of topological defects in the latter. The color scheme denotes the topological charge—i.e., the deviation from a coordination number of six. (d) PDFs of $|\Psi_6|$ at $d = 0.1$ with increasing motility. As the system goes through the intermittent regime, the PDF goes from unimodal (solid), to bimodal (intermittent), and back to unimodal (liquid).

form grain boundaries and percolate the system [Figs. 3(c) and S11 [49]].

We locate the intermittent region in the phase diagram (Fig. 2) via two separate methods. First, given that there are large fluctuations in $|\Psi_6|$ in this region, we identify states to be intermittent if both the standard error of $|\Psi_6|$ and $\bar{D}_{\mathrm{eff}}$ are above 0.0005. Second, we binarize the time series of $\langle|\Delta N_{\mathrm{nn}}|\rangle$ and map each time point to either zero (solid) or unity (liquid). For a time series to be intermittent, we require a minimum of two jumps between the states, and a large enough fraction of time spent in either state. Both methods converge and pinpoint a similar parameter region to be intermittent. Further, this region shrinks with increasing N (see Figs. S8 and S10 [49]). This suggests that intermittence arises because the solid-liquid transition is first order like at low deformability, so that coexistence between the two phases is expected at criticality. The first order character is also supported by finite size scaling of $|\Psi_6| = N^{\zeta} f(pN^{\nu})$ at low d, where $p = \mathrm{Pe}/\mathrm{Pe}^{*} - 1$ and $\zeta = -0.044(3)$, computed for systems up to 900 cells (see Fig. S12 [49]).

As anticipated, and clear from the phase diagram, the intermittent phase is only present at low deformability, when cells overlap. A possible mechanism through which cell overlap might affect the nature of the transition is the following. When cells are highly deformable and do not overlap with their neighbors, they can escape the local cage in which they are trapped by squeezing through their neighbors. These cage escapes lead to neighbor exchanges, hence to fluidification. On the other hand, if cells are not deformable but can overlap, moving a cell is similar to inserting or moving a coin on a substrate crowded with other coins (as in a "coin-pusher" arcade game). In this case, motion of the coin can either result in simple coin overlap or layering and no motion, or in the collective motion of a raft of coins. The coexistence of different scenarios (overlap or collective motion) may underlie the onset of intermittence in our simulations, and the first-order-like nature of the solid-liquid transition in the low deformability regime. We note a first-order-like glass-to-liquid transition has also been found in systems of active soft disks [55].

Finally, we analyze the relation between defects in the bond-orientational order and cell overlap. Experiments with monolayers of progenitor stem cells [56] have shown that these systems can be viewed as active nematics, and that topological defects in the nematic order correlate with the location of cell extrusion and death. Similar behavior has been obtained in MDCK (Madin Darby canine kidney) cells [48,57]. On the other hand, nematic order is often not readily apparent in epithelia, where cells are typically not elongated, and extrusion is presumably associated with high local overlap of a cell with its neighbors [43]. Our work offers an alternative interpretation that correlates cell extrusion not with defects in nematic order, but with cell overlap and associated structural defects in cell packing.

Defects in the hexagonal lattice formed by the cell centers in the ordered solid state are five- and sevenfold

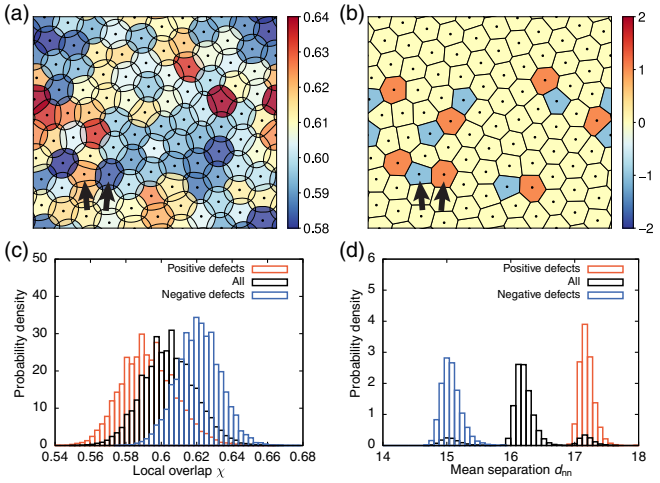

FIG. 4. Correlation between local overlap and defects at $(d, \mathrm{Pe}) = (0.1, 2.4)$. (a) Simulation snapshot. Color denotes the degree of local overlap–i.e., the fraction of a cell's area overlapped by other cells, which is given by $\chi_i = A_i^{-1} \int_{\Omega_i} d^2\boldsymbol{r}\chi_i(\boldsymbol{r})$, where Ω_i is the region where $\phi_i > 1$ and A_i is its area. (b) Voronoi tessellation of (a), colored by the topological charge of each cell [see Fig. 3(c)]. Black arrows point to the same two cells with defects in (a) and (b) to highlight that cells with fivefold disclinations have higher local overlap than those with sevenfold disclinations. (c) PDFs of the local overlap for different defect types. (d) PDFs of the mean separation d_{nn} of a cell from its nearest neighbors for different defect types.

disclinations and correspond to pentagonal and heptagonal cells, respectively, in the associated Voronoi tessellation [58]. They are readily identified in the cell packing, as shown in Figs. 4(a) and 4(b). We quantify the local overlap of the ith cell by computing the field $\chi_i(\boldsymbol{r}) \equiv \sum_{j=1}^{N} H[\phi_i(\boldsymbol{r}) - 1]H[\phi_j(\boldsymbol{r}) - 1]$, with H the Heaviside function. We then search for correlations between defects and overlap by recording both overlap and coordination number for each cell, and constructing the PDFs for the local overlap for pentagonal and heptagonal cells, as well as for the entire cell population [Fig. 4(c)]. The PDFs show that pentagons experience, on average, more overlap with respect to other cells. This can be understood by noting that, while all cells have approximately the same area [Fig. 4(a)], fivefold coordinated particles have a smaller mean distance to their neighbors [Fig. 4(d)]. Hence cell overlap is largest at fivefold defects, suggesting that these may be likely loci of cell extrusion, which is known that can be triggered by cell crowding. Our results suggest that cell extrusions in cell monolayers are likely to occur in the intermittent regime or near the solid-liquid transition, and may originate near fivefold coordinated cells.

In summary, we have used a multiphase field model to explore the effect of overlap and motility on the solid-liquid transition in confluent monolayers of active deformable cells. Melting is triggered by increasing motility and/or deformability, which promotes fluidification by allowing

cells to squeeze past their neighbors. We have shown that overlap strongly affects the nature of the melting transition in the monolayer. Specifically, when cells overlap rather than deform, the solid-liquid transition changes from continuous to first order like, and it is accompanied by an intermediate intermittent regime in which the monolayer alternates between solid and liquid states. This intermittent phase could be relevant to morphological processes that require periodic fluidization to restructure the tissue. We have also found a correlation between the location of topological defects in cell packing and fluctuations in local cell overlap, which suggests that cellular extrusion could be linked to the presence of these defects. Extrusion is an important process in epithelial tissues required for proper biological functioning. While it is normally thought that extrusion is determined by biochemical signaling, recent experiments have suggested a correlation between extrusion and topological defects in the orientational order of elongated or spindle-like cells. Here we suggest an alternative, possibly more general, correlation between extrusion and topological defects in the structure of cell packings that applies even when cells are not elongated.

From a theoretical point of view, it would be of interest to ask whether our active monolayers of deformable cells also exhibit a hexatic phase, which has been recently found in high-density suspensions of active Brownian particles [33,59]. Addressing this question will require simulations of much larger systems.

This work was supported by the National Science Foundation Grants No. DMR-1609208 (B. L. and M. C. M.) and No. PHY-1748958 (KITP). B. L. and M. C. M. would like to acknowledge the hospitality of KITP, where some of this work was done. M. C. acknowledges the Carnegie Trust for the Universities of Scotland for PhD studentship funding. Use was made of computational facilities purchased with funds from the National Science Foundation (CNS-1725797) and administered by the Center for Scientific Computing (CSC). The CSC is supported by the California NanoSystems Institute and the Materials Research Science and Engineering Center (MRSEC; NSF DMR-1720256) at UC Santa Barbara.

B. L. and M. C. contributed equally to this work.

*Corresponding author.
baloewe@uc.cl

[1] M. Chuai, D. Hughes, and C. J. Weijer, Collective epithelial and mesenchymal cell migration during gastrulation, Curr. Genomics **13**, 267 (2012).

[2] M. Poujade, E. Grasland-Mongrain, A. Hertzog, J. Jouanneau, P. Chavrier, B. Ladoux, A. Buguin, and P. Silberzan, Collective migration of an epithelial monolayer in response to a model wound, Proc. Natl. Acad. Sci. U.S.A. **104**, 15988 (2007).

[3] A. Haeger, M. Krause, K. Wolf, and P. Friedl, Cell jamming: Collective invasion of mesenchymal tumor cells imposed by tissue confinement, Biochim. Biophys. Acta **1840**, 2386 (2014).

[4] J. P. Thiery, Epithelial–mesenchymal transitions in tumour progression, Nat. Rev. Cancer **2**, 442 (2002).

[5] E. W. Thompson and D. F. Newgreen, Carcinoma invasion and metastasis: A role for epithelial-mesenchymal transition?, Cancer Res. **65**, 5991 (2005).

[6] J. A. Mitchel, A. Das, M. J. O'Sullivan, I. T. Stancil, S. J. DeCamp, S. Koehler, J. P. Butler, J. J. Fredberg, M. A. Nieto, D. Bi, and J.-A. Park, The unjamming transition is distinct from the epithelial-to-mesenchymal transition, bioRxiv, 665018 (2019).

[7] J. P. Thiery, H. Acloque, R. Y. Huang, and M. A. Nieto, Epithelial-mesenchymal transitions in development and disease, Cell **139**, 871 (2009).

[8] P. Friedl and D. Gilmour, Collective cell migration in morphogenesis, regeneration and cancer, Nat. Rev. Mol. Cell Biol. **10**, 445 (2009).

[9] T. E. Angelini, E. Hannezo, X. Trepat, M. Marquez, J. J. Fredberg, and D. A. Weitz, Glass-like dynamics of collective cell migration, Proc. Natl. Acad. Sci. U.S.A. **108**, 4714 (2011).

[10] K. D. Nnetu, M. Knorr, J. Käs, and M. Zink, The impact of jamming on boundaries of collectively moving weak-interacting cells, New J. Phys. **14**, 115012 (2012).

[11] J.-A. Park *et al.*, Unjamming and cell shape in the asthmatic airway epithelium, Nat. Mater. **14**, 1040 (2015).

[12] S. Garcia, E. Hannezo, J. Elgeti, J. F. Joanny, P. Silberzan, and N. S. Gov, Physics of active jamming during collective cellular motion in a monolayer, Proc. Natl. Acad. Sci. U.S.A. **112**, 15314 (2015).

[13] C. Malinverno *et al.*, Endocytic reawakening of motility in jammed epithelia, Nat. Mater. **16**, 587 (2017).

[14] L. Atia, D. Bi, Y. Sharma, J. A. Mitchel, B. Gweon, S. A. Koehler, S. J. DeCamp, B. Lan, J. H. Kim, R. Hirsch, A. F. Pegoraro, K. H. Lee, J. R. Starr, D. A. Weitz, A. C. Martin, J.-A. Park, J. P. Butler, and J. J. Fredberg, Geometric constraints during epithelial jamming, Nat. Phys. **14**, 613 (2018).

[15] A. Mongera, P. Rowghanian, H. J. Gustafson, E. Shelton, D. A. Kealhofer, E. K. Carn, F. Serwane, A. A. Lucio, J. Giammona, and O. Campàs, A fluid-to-solid jamming transition underlies vertebrate body axis elongation, Nature (London) **561**, 401 (2018).

[16] F. Graner and J. A. Glazier, Simulation of Biological Cell Sorting Using a Two-Dimensional Extended Potts Model, Phys. Rev. Lett. **69**, 2013 (1992).

[17] T. Nagai and H. Honda, A dynamic cell model for the formation of epithelial tissues, Philos. Mag. B **81**, 699 (2001).

[18] D. B. Staple, R. Farhadifar, J.-C. Röper, B. Aigouy, S. Eaton, and F. Jülicher, Mechanics and remodelling of cell packings in epithelia, Eur. Phys. J. E **33**, 117 (2010).

[19] A. G. Fletcher, M. Osterfield, R. E. Baker, and S. Y. Shvartsman, Vertex models of epithelial morphogenesis, Biophys. J. **106**, 2291 (2014).

[20] D. Bi, J. H. Lopez, J. M. Schwarz, and M. L. Manning, A density-independent rigidity transition in biological tissues, Nat. Phys. **11**, 1074 (2015).

[21] B. Li and S. X. Sun, Coherent motions in confluent cell monolayer sheets, Biophys. J. **107**, 1532 (2014).
[22] D. Bi, X. Yang, M. C. Marchetti, and M. L. Manning, Motility-Driven Glass and Jamming Transitions in Biological Tissues, Phys. Rev. X **6**, 021011 (2016).
[23] E. Teomy, D. A. Kessler, and H. Levine, Confluent and nonconfluent phases in a model of cell tissue, Phys. Rev. E **98**, 042418 (2018).
[24] L. Yan and D. Bi, Multicellular Rosettes Drive Fluid-solid Transition in Epithelial Tissues, Phys. Rev. X **9**, 011029 (2019).
[25] Y.-W. Li and M. P. Ciamarra, Role of cell deformability in the two-dimensional melting of biological tissues, Phys. Rev. Mater. **2**, 045602 (2018).
[26] M. Durand and J. Heu, Thermally Driven Order-Disorder Transition in Two-Dimensional Soft Cellular Systems, Phys. Rev. Lett. **123**, 188001 (2019).
[27] F. Giavazzi, M. Paoluzzi, M. Macchi, D. Bi, G. Scita, M. L. Manning, R. Cerbino, and M. C. Marchetti, Flocking transitions in confluent tissues, Soft Matter **14**, 3471 (2018).
[28] D. L. Barton, S. Henkes, C. J. Weijer, and R. Sknepnek, Active vertex model for cell-resolution description of epithelial tissue mechanics, PLoS Comput. Biol. **13**, e1005569 (2017).
[29] M. Chiang and D. Marenduzzo, Glass transitions in the cellular Potts model, Europhys. Lett. **116**, 28009 (2016).
[30] M. Engel, J. A. Anderson, S. C. Glotzer, M. Isobe, E. P. Bernard, and W. Krauth, Hard-disk equation of state: First-order liquid-hexatic transition in two dimensions with three simulation methods, Phys. Rev. E **87**, 042134 (2013).
[31] S. C. Kapfer and W. Krauth, Two-Dimensional Melting: From Liquid-Hexatic Coexistence to Continuous Transitions, Phys. Rev. Lett. **114**, 035702 (2015).
[32] A. Hajibabaei and K. S. Kim, First-order and continuous melting transitions in two-dimensional Lennard-Jones systems and repulsive disks, Phys. Rev. E **99**, 022145 (2019).
[33] P. Digregorio, D. Levis, L. F. Cugliandolo, G. Gonnella, and I. Pagonabarraga, Clustering of topological defects in two-dimensional melting of active and passive disks, arXiv:1911.06366.
[34] Y. Saito, Melting of Dislocation Vector Systems in Two Dimensions, Phys. Rev. Lett. **48**, 1114 (1982).
[35] S. T. Chui, Grain-boundary theory of melting in two dimensions, Phys. Rev. B **28**, 178 (1983).
[36] J. M. Kosterlitz and D. J. Thouless, Ordering, metastability and phase transitions in two-dimensional systems, J. Phys. C **6**, 1181 (1973).
[37] B. I. Halperin and D. R. Nelson, Theory of Two-Dimensional Melting, Phys. Rev. Lett. **41**, 121 (1978).
[38] D. R. Nelson, Study of melting in two dimensions, Phys. Rev. B **18**, 2318 (1978).
[39] A. P. Young, Melting and the vector Coulomb gas in two dimensions, Phys. Rev. B **19**, 1855 (1979).
[40] J. G. Dash, History of the search for continuous melting, Rev. Mod. Phys. **71**, 1737 (1999).
[41] U. Gasser, Crystallization in three- and two-dimensional colloidal suspensions, J. Phys. Condens. Matter **21**, 203101 (2009).
[42] R. Etournay, M. Popović, M. Merkel, A. Nandi, C. Blasse, B. Aigouy, H. Brandl, G. Myers, G. Salbreux, F. Jülicher, and S. Eaton, Interplay of cell dynamics and epithelial tension during morphogenesis of the *Drosophila* pupal wing, eLife **4**, e07090 (2015).
[43] G. T. Eisenhoffer, P. D. Loftus, M. Yoshigi, H. Otsuna, C.-B. Chien, P. A. Morcos, and J. Rosenblatt, Crowding induces live cell extrusion to maintain homeostatic cell numbers in epithelia, Nature (London) **484**, 546 (2012).
[44] M. I. Koster and D. R. Roop, Mechanisms regulating epithelial stratification, Annu. Rev. Cell Dev. Biol. **23**, 93 (2007).
[45] M. Nonomura, Study on multicellular systems using a phase field model, PLoS One **7**, e33501 (2012).
[46] B. Palmieri, Y. Bresler, D. Wirtz, and M. Grant, Multiple scale model for cell migration in monolayers: Elastic mismatch between cells enhances motility, Sci. Rep. **5**, 11745 (2015).
[47] M. Foglino, A. N. Morozov, O. Henrich, and D. Marenduzzo, Flow of Deformable Droplets: Discontinuous Shear Thinning and Velocity Oscillations, Phys. Rev. Lett. **119**, 208002 (2017).
[48] R. Mueller, J. M. Yeomans, and A. Doostmohammadi, Emergence of Active Nematic Behavior in Monolayers of Isotropic Cells, Phys. Rev. Lett. **122**, 048004 (2019).
[49] See the Supplemental Material at http://link.aps.org/supplemental/10.1103/PhysRevLett.125.038003, which contains additional details on the model and additional results complementing those shown in the main text, as well as Refs. [50,51].
[50] S. M. Bhattacharjee and F. Seno, A measure of data collapse for scaling, J. Phys. A **34**, 6375 (2001).
[51] W. H. Press, S. A. Teukolsky, W. T. Vetterling, and B. P. Flannery, *Numerical Recipes in C (2nd Ed.): The Art of Scientific Computing* (Cambridge University Press, USA, 1992).
[52] I. Pagonabarraga, A. J. Wagner, and M. E. Cates, Binary fluid demixing: The crossover region, J. Stat. Phys. **107**, 39 (2002).
[53] P. Romanczuk, M. Bär, W. Ebeling, B. Lindner, and L. Schimansky-Geier, Active Brownian particles, Eur. Phys. J. Special Topics **202**, 1 (2012).
[54] Y. Fily and M. C. Marchetti, Athermal Phase Separation of Self-Propelled Particles with No Alignment, Phys. Rev. Lett. **108**, 235702 (2012).
[55] Y. Fily, S. Henkes, and M. C. Marchetti, Freezing and phase separation of self-propelled disks, Soft Matter **10**, 2132 (2014).
[56] K. Kawaguchi, R. Kageyama, and M. Sano, Topological defects control collective dynamics in neural progenitor cell cultures, Nature (London) **545**, 327 (2017).
[57] T. B. Saw, A. Doostmohammadi, V. Nier, L. Kocgozlu, S. Thampi, Y. Toyama, P. Marcq, C. T. Lim, J. M. Yeomans, and B. Ladoux, Topological defects in epithelia govern cell death and extrusion, Nature (London) **544**, 212 (2017).
[58] M. J. Bowick and L. Giomi, Two-dimensional matter: Order, curvature and defects, Adv. Phys. **58**, 449 (2009).
[59] P. Digregorio, D. Levis, A. Suma, L. F. Cugliandolo, G. Gonnella, and I. Pagonabarraga, Full Phase Diagram of Active Brownian Disks: From Melting to Motility-Induced Phase Separation, Phys. Rev. Lett. **121**, 098003 (2018).